Anatase formation on titanium by two-step thermal oxidation

**Takuro Okazumi · Kyosuke Ueda · Kazuki Tajima ·
Nobuyuki Umetsu · Takayuki Narushima**

Abstract Two-step thermal oxidation of commercially
pure Ti was investigated with a focus on the formation
of anatase. A first-step treatment was conducted in Ar–
(0.1–20)%CO atmosphere at a temperature of 773–1173 K
for a holding time of 0 or 86.4 ks, and a subsequent sec-
ond-step treatment was conducted in air at 473–873 K for
0–86.4 ks. Titanium oxides and titanium oxycarbide were
obtained in the first step, with relative amounts depending
on heating temperature, holding time, and CO partial
pressure. An anatase-rich layer on Ti was obtained after
second-step treatment in air at 573–773 K in cases where
single-phase titanium oxycarbide formed in the first step.
Thus, the formation of single-phase titanium oxycarbide in
the first step and temperature control in the second step
were required for the formation of an anatase-rich layer.
The bonding strength of an anatase-rich layer with a
thickness of 0.5 μm was calculated to be around 90 MPa.
This study reveals the conditions under which an anatase-
rich layer with excellent adherence to Ti can be prepared
by thermal oxidation.

T. Okazumi · K. Ueda · N. Umetsu · T. Narushima (✉)
Department of Materials Processing, Graduate School of
Engineering, Tohoku University, 6-6-02 Aza Aoba, Aramaki,
Aoba-ku, Sendai 980-8579, Japan
e-mail: narut@material.tohoku.ac.jp

K. Tajima
Materials Research Institute for Sustainable Development,
National Institute of Advanced Industrial Science and
Technology (AIST), Nagoya 463-8560, Japan

Introduction

Titanium (Ti) and its alloys have excellent properties such as
high specific strength and high corrosion resistance and can
exhibit a wide range of mechanical properties depending on
alloy composition and thermomechanical treatments. Given
these advantages, they have been employed in aerospace and
military industries as well as chemical plants. More recently,
their use has been extended to applications such as bio-
medical implants, buildings, and sporting goods.

A layer of titanium dioxide (titania: TiO_2) affects the
surface properties of Ti. Previous studies have reported that
a TiO_2 layer formed on Ti improves corrosion resistance
[1, 2] and biocompatibility [3–10], in addition to providing
photocatalytic activity [11]. The polymorphic phases of
TiO_2 are tetragonal rutile, tetragonal anatase, and ortho-
rhombic brookite. On a macroscopic scale, rutile is ther-
modynamically stable relative to anatase and brookite [12,
13]. However, the relative stability of these phases depends
on particle size [13, 14], and anatase becomes the stable
phase under conditions of small particle size. In biomedical
research, it has been reported that the formation of anatase
phase on Ti implants improves their bone compatibility
[5–10]. In addition, anatase [15] as well as anatase–rutile
[16] and anatase–brookite [17, 18] composites are known
to exhibit high levels of photocatalytic activity.

Anatase-rich layers on Ti have previously been prepared
by methods based on vapor deposition [19, 20] or wet
processes [5–11, 21]. Vapor deposition is a relatively
expensive process, and the adherence of the TiO_2 layer
formed by wet processes is generally low. In contrast,
thermal oxidation is a simple and low-cost method to
prepare TiO_2 layers on Ti with excellent adherence and can
be applied to substrates with a complex geometry. There-
fore, controlling the TiO_2 phases on Ti by thermal

oxidation should contribute to expand the applications of Ti in biomedical and photocatalytic fields.

During the thermal oxidation of Ti, rutile phase has been reported as the main oxidation product [22, 23], and a few studies have reported the formation of anatase as the minor phase [24, 25]. Borgioli et al. [24] reported the formation of anatase as the minor phase (with rutile as the main phase) in the oxidized film on a Ti–6Al–4V alloy after glow-discharge processing in air at a total gas pressure of 0.01 atm. Lee and Park [25], using oxidation in a wet oxygen atmosphere for 10.8 ks at 683 K in combination with post-annealing in air at 773 K, showed formation of a Ti_5O_7/anatase layer (with Ti_5O_7 as the main phase) on a magnetron-sputtered Ti thin film. However, the formation of an anatase-rich layer on Ti by thermal oxidation has not been reported thus far.

In this study, we developed a two-step thermal oxidation method consisting of a first step in Ar–CO atmosphere and a second step in air for forming anatase on Ti and investigated the effects of process parameters in both steps on the resultant products and their adherence to Ti.

Experimental

Commercially pure (CP) Ti plates (JIS Gr.2) with dimensions of $10^L \times 10^B \times 2^T$ mm were used as specimens for the thermal oxidation treatments. The CP Ti plates were mirror-polished (Ra < 0.05 μm). Subsequently, they were ultrasonically cleaned in ultrapure water and ethanol for 0.3 ks each, and then dried at room temperature before the thermal oxidation treatments.

The first step was conducted in an atmosphere of Ar–(0.1–20)%CO (primarily Ar–1%CO) using an electric resistance furnace with a silica reaction tube (inner diameter: 4.6×10^{-2} m). The flow rate of Ar–CO gas was 6.7×10^{-6} m³ s⁻¹ at 1 atm and 273.15 K. The total gas pressure was 1 atm. The gas atmosphere during the increases and decreases in specimen temperature was the same as that during holding. The specimen temperature was increased to a specified value at a rate of 8.3 K s⁻¹ and cooled in the furnace at the same rate after holding at a specified temperature. The treatment temperature varied between 673 and 1173 K. The holding time for the treatment in the first step was 0 or 86.4 ks. A holding time of 0 ks implies that the specimens were cooled immediately after the specimen temperature reached a specified value. A Ti sponge was placed at the gas inlet side of the specimen in the tube furnace to remove the oxidant impurities in the Ar–CO gas.

Following the first-step treatment, the second step was conducted in air at 473–873 K for 0–86.4 ks using an electric resistance muffle furnace (KBF828N, Koyo Thermo Systems Co, Ltd.). The rate at which the specimen temperature increased or decreased in the second step was 8.3 K s⁻¹ in both cases.

After the first or second step, the reaction layer on Ti was analyzed by $\alpha - 2\theta$ X-ray diffraction (XRD: RU-200B, CuKα, Rigaku) with an incident angle of 0.3° and $\theta - 2\theta$ XRD (D8 ADVANCE, CuKα, Bruker AXS). Cross sections of the reaction layer were observed by scanning electron microscopy (SEM, PHILIPS, XL30FEG) and transmission electron microscopy (TEM: EM-2100, JEOL and H-800, Hitachi). Chemical bonding in the reaction layer was evaluated using X-ray photoelectron spectroscopy (XPS: Sigma Probe, Thermo Scientific).

The bonding strength between Ti and the reaction layer formed by the two-step treatment was evaluated using a mechanical strength tester (Romulus IV, Quad Group). An aluminum (Al) stud with epoxy glue (P/N 901106, Quad Group) was attached to the surface of the reaction layer on Ti. The maximum load for the pulling test with the Al stud was recorded and used to evaluate the bonding strength between the reaction layer and Ti ($N = 5$). Details of the procedures for evaluating bonding strength have been reported elsewhere [26].

Results

Figure 1 shows the $\alpha - 2\theta$ and $\theta - 2\theta$ XRD patterns of the reaction layer after the first step in Ar–1%CO atmosphere at 1073 K for 0 ks, along with the standard patterns of TiC (JCPDS card no. 32-1383) and α-Ti (JCPDS card no. 44-1294). The XRD pattern of the reaction layer was close to the standard pattern of TiC, although the reflections shifted toward higher angles. The XPS spectra for Ti 2p, C 1s, and O 1s of the reaction layer as a function of the duration of Ar ion etching are displayed in Fig. 2. The presence of both Ti–C and Ti–O bonds was confirmed. From the results of XRD and XPS analyses, the phase in the reaction layer can be concluded to be titanium oxycarbide, $TiC_{1-x}O_x$. It has been reported that the substitution of oxygen for carbon in TiC decreases its lattice constant [27]; this is consistent with the shift in the reflections observed in this study (Fig. 1). The intensity of the Ti–C bonding peaks in Fig. 2a and b increased with the Ar ion etching time, indicating that the value of x in $TiC_{1-x}O_x$ decreased across the reaction layer from the surface to Ti. SEM observations revealed that the thickness of the $TiC_{1-x}O_x$ layer formed by heating at 1073 K for 0 ks was around 0.2 μm (Fig. 3).

The reaction products after the first- and second-step treatments are summarized in Fig. 4. The first-step treatment was carried out under conditions of Ar–1%CO
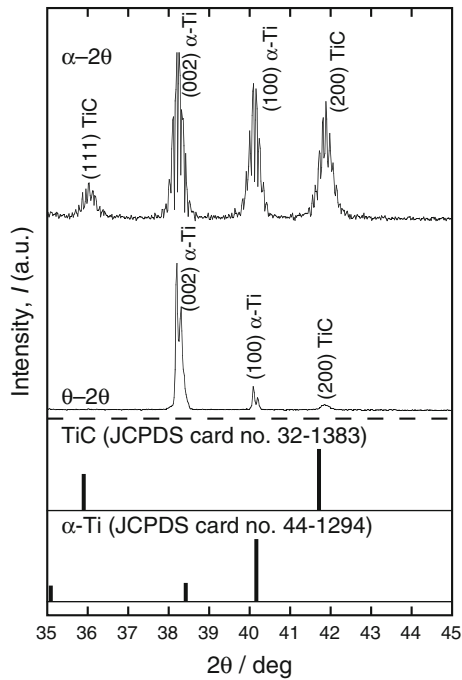
Fig. 1 $\alpha - 2\theta$ and $\theta - 2\theta$ XRD patterns of reaction layer after first step and JCPDS reference patterns of TiC (card no. 32-1383) and α-Ti (card no. 44-1294)
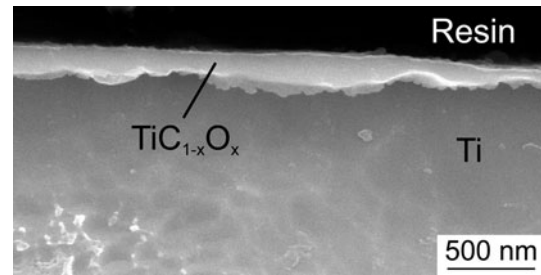

Fig. 3 Cross section of reaction layer ($TiC_{1-x}O_x$) after first step in Ar–1%CO atmosphere at 1073 K for 0 ks

atmosphere at 673–1173 K for 0 (Fig. 4a) or 86.4 ks (Fig. 4b). After the first-step treatment, the subsequent second-step treatment was carried out under the same conditions: air atmosphere, temperature of 773 K, and holding time of 86.4 ks. In Fig. 4, the phase fraction in the reaction products is expressed in terms of the relative intensities of the strongest peaks of the phases in the $\alpha - 2\theta$ XRD patterns of the reaction layers. The $TiC_{1-x}O_x$

phase was obtained over a wide range of conditions in the first step. Single-phase $TiC_{1-x}O_x$ was obtained after treatment at higher temperatures. A rutile phase was detected at lower treatment temperatures. The titanium suboxides Ti_6O_{11} and Ti_5O_9 were formed at a treatment temperature of 1173 K and holding time of 86.4 ks. After the second step, an anatase-rich layer was detected in cases where single-phase $TiC_{1-x}O_x$ was formed in the first step.

Figure 5 shows the $\alpha - 2\theta$ and $\theta - 2\theta$ XRD patterns of the reaction layers after the second step in air at 773 K for various holding times under the same first-step conditions (in Ar–1%CO atmosphere at 1073 K for 0 ks). An anatase-rich layer was detected even after immediate cooling (holding time: 0 ks) in the second step. The anatase-to-rutile peak intensity ratio decreased with increasing holding time in the second step. In the $\alpha - 2\theta$ XRD patterns, this ratio was higher than in the $\theta - 2\theta$ XRD patterns. This may indicate that the outer part of the reaction layer is anatase-rich relative to the inner part. The cross sections of anatase-rich layers formed during the second step in air at 773 K for 0 ks after the first step in Ar–1%CO atmosphere
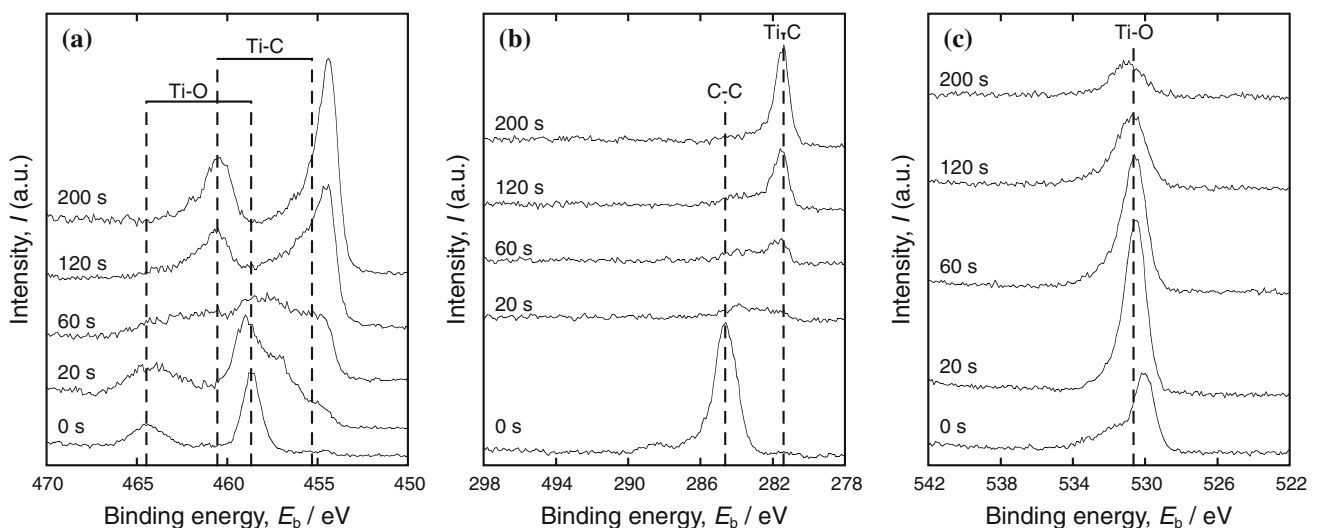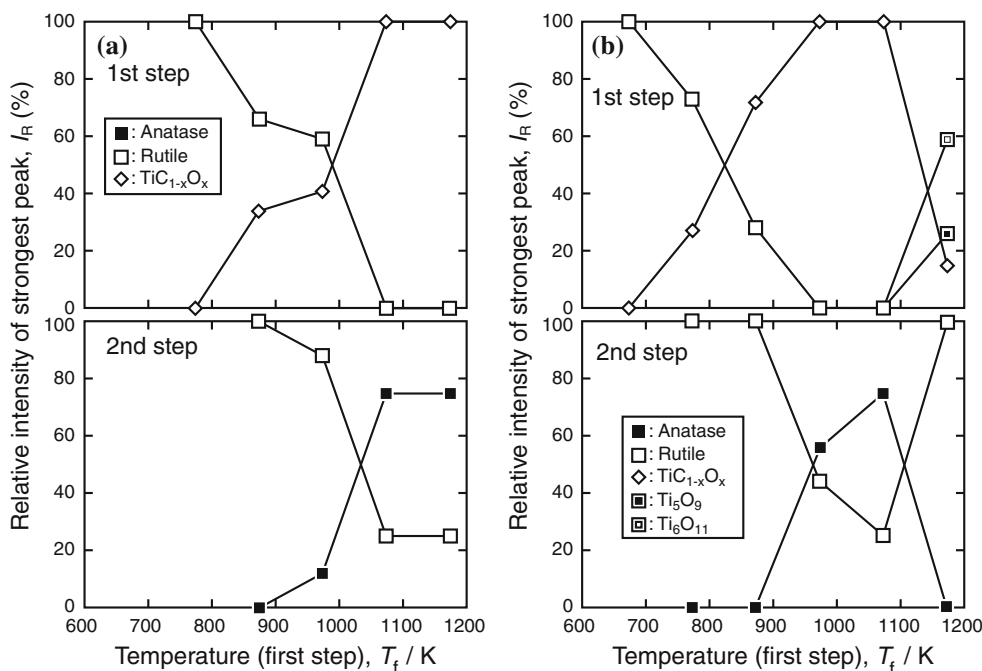

Fig. 2 XPS spectra for a Ti 2p, b C 1s, and c O 1s of reaction layer after first step in Ar–1%CO atmosphere at 1073 K for 0 ks as a function of duration of Ar ion etching up to 200 s

Fig. 4 Relative intensities of strongest peaks of phases in $\alpha - 2\theta$ XRD patterns of reaction layers obtained after first-step and second-step treatments. The holding periods of time in the first step are **a** 0 and **b** 86.4 ks

for 0 ks at 1073 and 1173 K are demonstrated in Fig. 6a and b, respectively. The thicknesses of the reaction layers for first-step temperatures of 1073 and 1173 K were around 0.5 and 1.5 μm, respectively. Figure 7a shows the TEM image of a cross section of the reaction layer on Ti after the two-step treatment, where the first step was in Ar–1%CO atmosphere at 1073 K for 0 ks and the second step was in air at 773 K for 86.4 ks. Small grains were observed in the reaction layer. The electron diffraction pattern of a selected area of the reaction layer is shown in Fig. 7b. As schematically illustrated in Fig. 7c, both patterns of rutile and anatase were detected.

Figure 8a and b depicts the $\alpha - 2\theta$ and $\theta - 2\theta$ XRD patterns of the reaction layers, respectively, after the second step in air for 86.4 ks at various temperatures. The first step was conducted in Ar–1%CO atmosphere at 1073 K for 0 ks. The formation of anatase phase was detected after the second step at temperatures ranging from 573 to 773 K. On the other hand, single-phase rutile was obtained after the second step at 873 K. At 473 K, $TiC_{1-x}O_x$ was still the main phase. Figure 9a and b shows the $\alpha - 2\theta$ XRD patterns of the reaction layers after the first step at 1073 K for 0 ks under various CO partial pressures in Ar–CO atmosphere and after the second step in air at 773 K for 86.4 ks, respectively. A weak reflection for rutile was observed after the first step at high CO partial pressures (e.g., in atmospheres of Ar–20%CO and Ar–10%CO), which led to rutile-rich layers after the second step.

The bonding strength of the anatase-rich layer (first step in Ar–1%CO at 1073 K for 0 ks and second step in air at 773 K for 86.4 ks) with a thickness of 0.5 μm (see Figs. 6a and 7a)

was calculated to be around 90 MPa. The specimen surface after the adherence test is shown in Fig. 10. The TiO_2 layer and epoxy glue as well as Ti surface can be detected on the specimen surface, indicating that detachment of the reaction layer occurred at the TiO_2/glue, glue/Al stud, and Ti/TiO_2 layer interfaces and in the interior of the epoxy glue. Therefore, it is improbable that values of around 90 MPa reflect the bonding strength of the reaction layer to Ti. However, it can be estimated that the bonding strength of the anatase-rich layer to Ti is greater than 90 MPa.

Discussion

Single-phase $TiC_{1-x}O_x$ was obtained after the first-step treatment in Ar–1%CO atmosphere at high temperatures. $TiC_{1-x}O_x$ appears to be a stable phase under these conditions. Few thermodynamic data on titanium oxycarbide have been reported thus far. The temperature dependence of the standard Gibbs free energy of Ti_2CO formation ($\Delta G_T^\circ(Ti_2CO)$) was reported by Maitre et al. [28], who measured the specific heat of Ti_2CO. Using their data on $\Delta G_T^\circ(Ti_2CO)$ in Eq. (1), the potential diagram of the Ti–C–O system at 1100 K was constructed as Fig. 11.

$$2Ti(s) + C(s) + 1/2O_2(g) = Ti_2CO(s)$$

$$\Delta G_T^\circ(Ti_2CO) = -999.4 + 0.2241T \ (kJ \ mol^{-1})$$
$$(T: 298 - 1800 \ K) \qquad (1)$$

The standard Gibbs free energy for $TiC_{1-x}O_x$ ($0 \le x \le 0.33$) formation at 1580 K ($\Delta G_{1580}^\circ(TiC_{1-x}O_x)$)
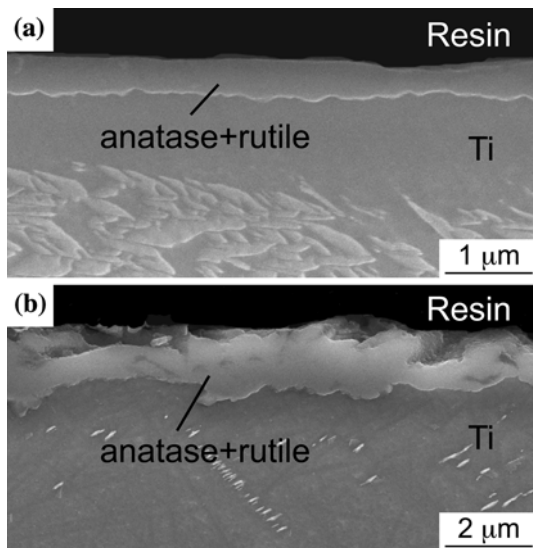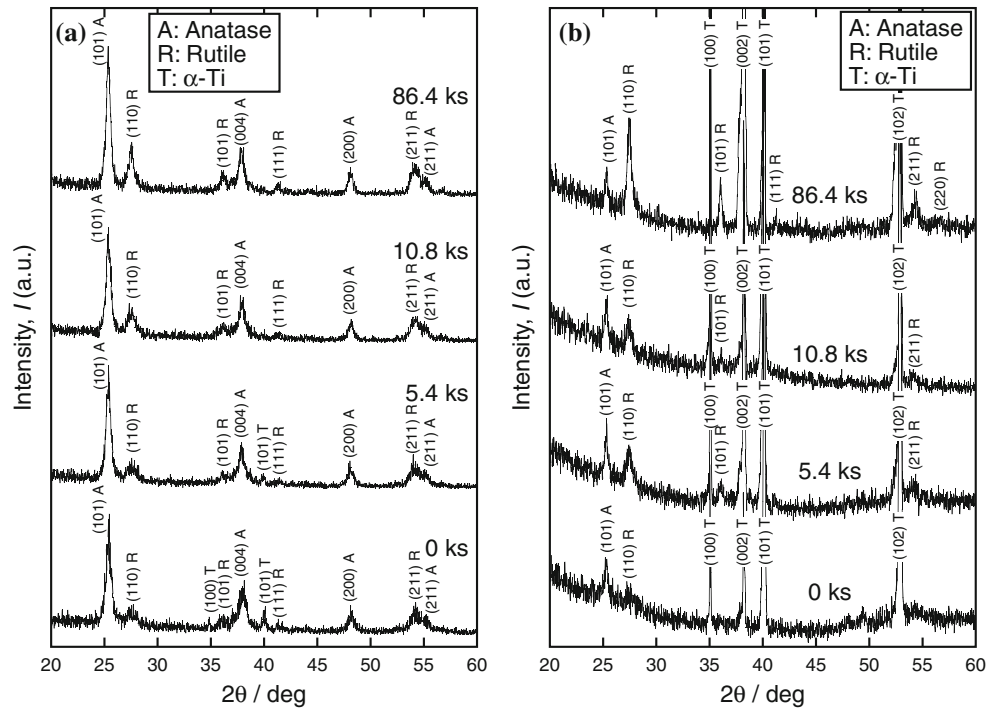
Fig. 6 Cross sections of reaction layers (anatase + rutile) formed during second-step treatment in air at 773 K for 86.4 ks after first-step treatment at **a** 1073 K and **b** 1173 K in an Ar–1%CO atmosphere for 0 ks
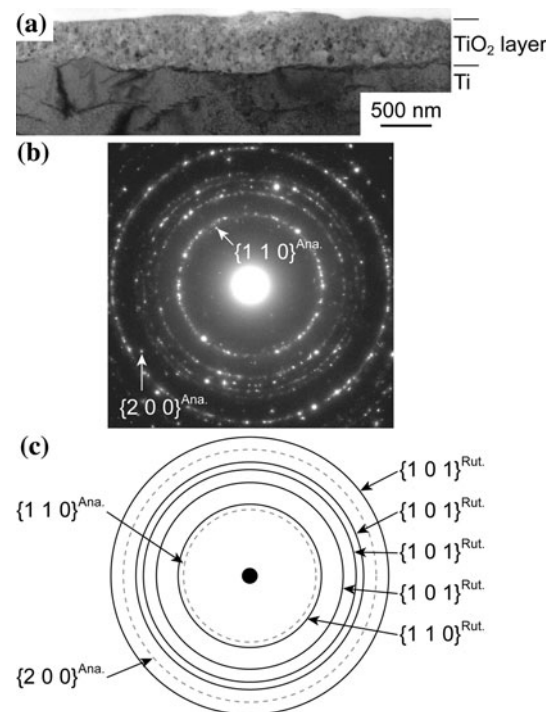

Fig. 7 **a** TEM image, **b** electron diffraction pattern of selected area, and **c** schematic diagram of diffraction pattern for reaction layer after two-step treatment

was reported by Ouensanga [29], and the values of $\Delta G^{\circ}_{1580}(\text{TiC}_{1-x}\text{O}_x)$ were suggested to change linearly when x in $\text{TiC}_{1-x}\text{O}_x$ changes from 0.04 to 0.33 [30, 31]. In constructing Fig. 11, the change in the composition of $\text{TiC}_{1-x}\text{O}_x$ was ignored. The standard Gibbs free energies for the formation of other substances are given by NIST-JANAF thermochemical tables [32]. The relationship between carbon activity (a_C) and oxygen partial pressure

(P_{O_2}) at a CO partial pressure (P_{CO}) of 0.01 atm—the main experimental condition used in the first step of this study is represented in Fig. 11. The Ti_2CO phase was suggested to be stable under the conditions of first-step treatment at a sufficiently low P_{O_2}.

Fig. 8 Variation in reaction layer phases with respect to temperature of second step in air for 86.4 ks after first step in Ar–1%CO atmosphere at 1073 K for 0 ks. **a** and **b** show the $\alpha - 2\theta$ and $\theta - 2\theta$ XRD patterns, respectively, of the reaction layer
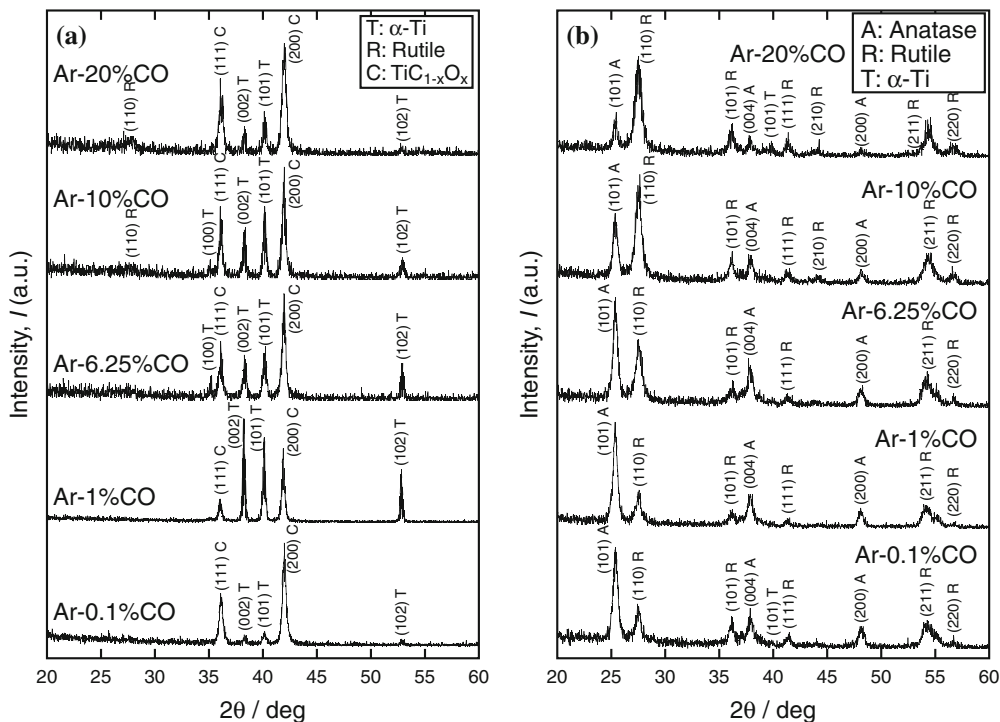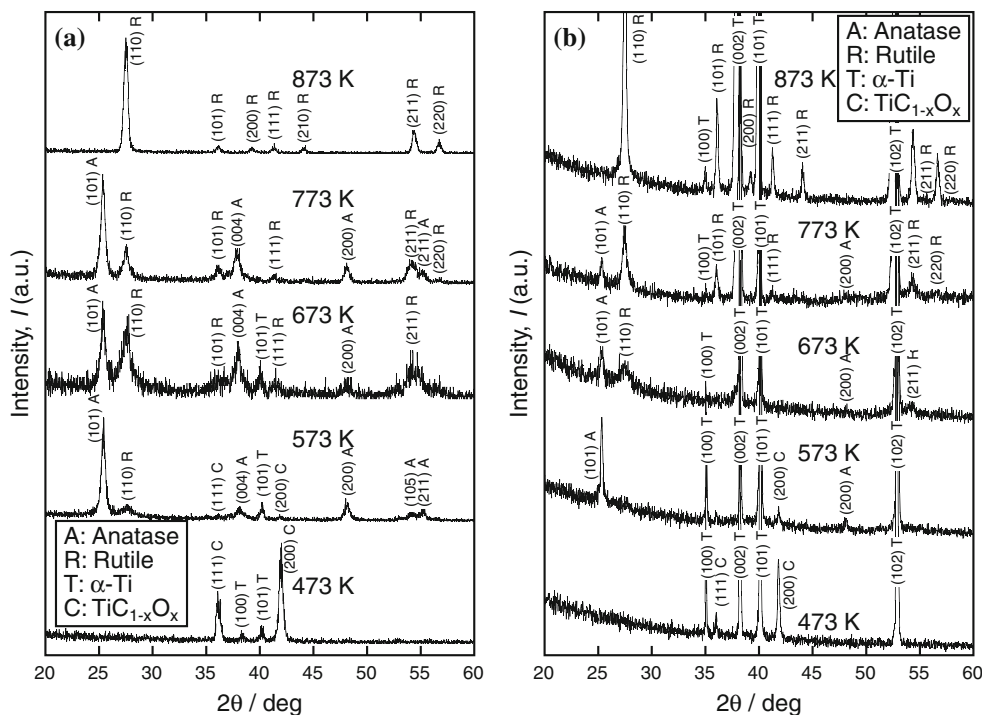

Fig. 9 $\alpha - 2\theta$ XRD patterns of reaction layer after **a** first step at various CO partial pressures in Ar–CO atmosphere and **b** subsequent second step in air at 773 K for 86.4 ks

Given that rutile phase was detected in the first step in Ar–1%CO atmosphere at 773–973 K for 0 ks (Fig. 4a), it might have been present on Ti before the specimen temperature reached 1073 K. Therefore, it is possible that the reduction of rutile phase to the $TiC_{1-x}O_x$ phase occurred in Ar–1%CO atmosphere. This reduction from rutile to $TiC_{1-x}O_x$ phase is apparently achieved by the following reactions via Magnéli oxides (Ti_nO_{2n-1}) [33].

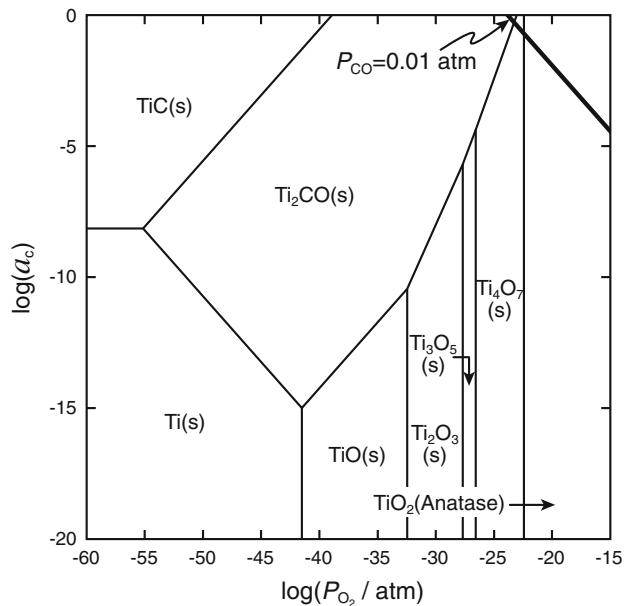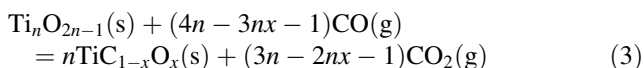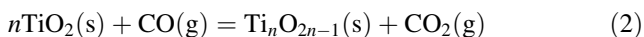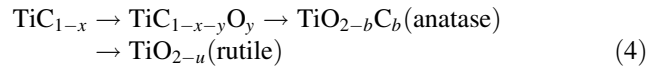**Fig. 10** SEM image of specimen surface after adherence test

Fig. 11 Potential diagram of Ti–C–O system at 1100 K

$$nTiO_2(s) + CO(g) = Ti_nO_{2n-1}(s) + CO_2(g) \qquad (2)$$

$$Ti_nO_{2n-1}(s) + (4n - 3nx - 1)CO(g)$$
$$= nTiC_{1-x}O_x(s) + (3n - 2nx - 1)CO_2(g) \qquad (3)$$

The oxide phases of $Ti_6O_{11} + Ti_5O_9$ and TiO_2 were detected as the main products in the reaction layer after the first-step treatments in Ar–1%CO atmosphere at 1173 K for 86.4 ks and at 673–873 K, respectively. In the first step, rutile phase was found with $TiC_{1-x}O_x$ at 1073 K under high P_{CO} (see Fig. 9a). Therefore, in order to obtain single-phase $TiC_{1-x}O_x$, it is necessary to control the heating temperature, holding time, and P_{CO} during the first-step treatment.

The formation of an anatase-rich layer was detected after the second-step treatment when single-phase $TiC_{1-x}O_x$ was formed in the first step. In thermal oxidation of Ti, rutile has been generally reported to be the dominant phase. On the other hand, in thermal oxidation of titanium carbide, the formation of anatase as the main phase has

been reported in the temperature range of 623–873 K [27, 34–36]. Shabalin et al. [27] presented an oxidation model of titanium carbide (TiC_{1-x}) coexisting with graphite in O_2 atmosphere;

$$TiC_{1-x} \rightarrow TiC_{1-x-y}O_y \rightarrow TiO_{2-b}C_b(anatase)$$
$$\rightarrow TiO_{2-u}(rutile) \qquad (4)$$

In their model, carbon is first substituted by oxygen to form titanium oxycarbide. Subsequently, carbon-containing anatase forms as substitution proceeds, after which rutile phase finally forms. In addition, it has been reported that a carbon coating on anatase suppresses the anatase-to-rutile transition at 973 K in N_2 atmosphere [37]. These reports indicate that the incorporation of carbon in TiO_2 stabilizes the anatase phase. Similar to the oxidation of titanium carbide, our results suggest that the carbon in $TiC_{1-x-y}O_y$ is incorporated into titanium oxide and stabilizes the ana-tase phase in air oxidation at temperatures of 573–773 K. At 873 K, however, the rutile but not the anatase phase formed via the oxidation of $TiC_{1-x-y}O_y$ in air (Fig. 8). At a high temperature of 873 K, all the carbon may have been oxidized to CO or CO_2 in air, thus allowing the transition from anatase to rutile to occur. The $TiC_{1-x-y}O_y$ phase was still observed after holding at 473 K for 86.4 ks, indicating that the oxidation reaction did not proceed in air. There-fore, temperature control in the second step is essential to obtain the anatase phase.

The bonding strength of the anatase-rich layer to Ti was very high (~ 90 MPa) compared to that of the anatase layer to NiTi prepared by the sol–gel technique and steam crystallization (~ 25 MPa) [38] and to that of ana-tase + rutile layer on Ti prepared by anodic oxidation (31.2–34.2 MPa) [39]. The two-step thermal oxidation method proposed in this study can be applied to the for-mation of an anatase-rich layer on Ti. In addition, the reaction rates in both the first and second steps appear to be high because reactions forming $TiC_{1-x}O_x$ and an anatase-rich layer were observed at 1073 and 773 K, respectively, for a holding time of 0 ks. The formation of an anatase-rich layer with excellent adherence to Ti by thermal oxidation may thus be effective for surface modification in biomed-ical and photocatalytic fields.

Conclusions

Two-step thermal oxidation of CP Ti involving a first step in Ar–CO atmosphere and a second step in air was inves-tigated with a focus on the formation of anatase phase, yielding the following results.

(1) $TiC_{1-x}O_x$ phase was obtained over a wide range of conditions in the first step, and single-phase $TiC_{1-x}O_x$

was obtained after treatment in Ar–0.1%CO and Ar–1%CO atmospheres at high temperatures.

(2) An anatase-rich layer with excellent adherence to Ti was obtained after second-step treatment in air at 573–773 K in cases where single-phase $TiC_{1-x}O_x$ formed in the first step. Therefore, formation of single-phase $TiC_{1-x}O_x$ in the first step and temperature control in the second step are required for preparing an anatase-rich layer.

References

1. Satoh H, Kamikubo F, Shimogori K (1986) Tetsu-to-Hagané 72:300
2. Sun C, Hui R, Qu W, Yick S, Sun C, Qian W (2010) J Mater Sci 45:6235. doi:10.1007/s10853-010-4718-7
3. Huang N, Yang P, Leng YX, Chen JY, Sun H, Wang J, Wang GJ, Ding PD, Xi TF, Leng Y (2003) Biomaterials 24:2177
4. Sugino A, Tsuru K, Hayakawa S, Kikuta K, Kawachi G, Osaka A, Ohtsuki C (2009) J Ceram Soc Jpn 117:515
5. Lin C-M, Yen S-K (2006) Mater Sci Eng C 26:54
6. Wu J-M, Hayakawa S, Tsuru K, Osaka A (2002) Thin Solid Films 414:283
7. Liang B, Fujibayashi S, Neo M, Tamura J, Kim H-M, Uchida M, Kokubo T, Nakamura T (2003) Biomaterials 24:4959
8. Yang X-F, Chen Y, Yang F, He F-M, Zhao S-F (2009) Dent Mater 25:473
9. Fujibayashi S, Nakamura T, Nishiguchi S, Tamura J, Uchida M, Kim H-M, Kokubo T (2001) J Biomed Mater Res 56:562
10. Zhao Z, Chen X, Chen A, Huo G, Li H (2009) J Mater Sci 44:6310. doi:10.1007/s10853-009-3869-x
11. Masahashi N, Mizukoshi Y, Senboshi S, Ohtsu N (2009) Appl Catal B 90:255
12. Zhang H, Banfield JF (2000) J Phys Chem B 104:3481
13. Zhang H, Banfield JF (1998) J Mater Chem 8:2073
14. Gouma PI, Mills MJ (2001) J Am Ceram Soc 84:619
15. Tanaka K, Capule MFV, Hisanaga T (1991) Chem Phys Lett 187:73
16. Kawahara T, Ozawa T, Iwasaki M, Tada H, Ito S (2003) J Colloid Interface Sci 267:377
17. Ozawa T, Iwasaki M, Tada H, Akita T, Tanaka K, Ito S (2005) J Colloid Interface Sci 281:510
18. Popa M, Diamandescu L, Vasiliu F, Teodorescu CM, Cosoveanu V, Baia M, Feder M, Baia L, Danciu V (2009) J Mater Sci 44:358. doi:10.1007/s10853-008-3147-3
19. Hirose F, Ito M, Kurita K (2008) Jpn J Appl Phys 47:5619
20. Chaiyakun S, Pokaipisit A, Limsuwan P, Ngotaworhai B (2009) Appl Phys A 95:579
21. Saji VS, Choe HC, Brantley WA (2009) J Mater Sci 44:3975. doi:10.1007/s10853-009-3542-4
22. Kusabiraki K, Kuroda N, Motohira I, Ooka T (1994) Tetsu-to-Hagané 80:155
23. Dong H, Li XY (2000) Mater Sci Eng A 280:303
24. Borgioli F, Galvanetto E, Fossati A, Pradelli G (2004) Surf Coat Technol 184:255
25. Lee K-S, Park I-S (2003) Scr Mater 48:659
26. Ueda K, Narushima T, Goto T, Katsube T, Nakagawa H, Kawamura H, Taira M (2007) Mater Trans 48:307
27. Shabalin IL, Roach DL, Shabalin LI (2008) J Eur Ceram Soc 28:3177
28. Maitre A, Cathalifaud P, Lefort P (1997) High Temp Mater Process 1:393
29. Ouensanga A (1981) J Less-Common Met 79:237
30. Bellucci A, Gozzi D, Latini A (2004) Solid State Ion 172:369
31. Kwon H, Kang S (2009) J Am Ceram Soc 92:272
32. Chase MW Jr (1998) NIST-JANAF thermochemical tables, 4th edn. ACS and AIP, New York
33. Shaviv R (1996) Mater Sci Eng A 209:345
34. Shimada S, Kozeki M (1992) J Mater Sci 27:1869. doi:10.1007/BF01107214
35. Irie H, Watanabe Y, Hashimoto K (2003) Chem Lett 32:772
36. Mitsuo A, Uchida S, Nihira N, Iwaki M (1998) Surf Coat Technol 103–104:98
37. Tsumura T, Kojitani N, Izumi I, Iwashita N, Toyoda M, Inagaki M (2002) J Mater Chem 12:1391
38. Chiu KY, Wong MH, Cheng FT, Man HC (2007) Appl Surf Sci 253:6762
39. Park Y-J, Shin K-H, Song H-J (2007) Appl Surf Sci 253:6013